# A volumetric model-based 2D to 3D registration method for measuring kinematics of natural knees with single-plane fluoroscopy

Tsung-Yuan Tsai, Tung-Wu Lu,[a] and Chung-Ming Chen
*Institute of Biomedical Engineering, National Taiwan University, No. 1, Sec. 1, Jen-Ai Road, Taipei 10051, Taiwan, Republic of China*

Mei-Ying Kuo
*Institute of Biomedical Engineering, National Taiwan University, No. 1, Sec. 1, Jen-Ai Road, Taipei 10051, Taiwan, Republic of China and Department of Physical Therapy, China Medical University, Taichung 40402, Taiwan, Republic of China*

Horng-Chaung Hsu
*Department of Orthopaedic Surgery, China Medical University Hospital, Taichung 40447, Taiwan, Republic of China*

(Received 14 July 2009; revised 8 December 2009; accepted for publication 7 January 2010; published 25 February 2010)

**Purpose:** Accurate measurement of the three-dimensional (3D) rigid body and surface kinematics of the natural human knee is essential for many clinical applications. Existing techniques are limited either in their accuracy or lack more realistic experimental evaluation of the measurement errors. The purposes of the study were to develop a volumetric model-based 2D to 3D registration method, called the weighted edge-matching score (WEMS) method, for measuring natural knee kinematics with single-plane fluoroscopy to determine experimentally the measurement errors and to compare its performance with that of pattern intensity (PI) and gradient difference (GD) methods.

**Methods:** The WEMS method gives higher priority to matching of longer edges of the digitally reconstructed radiograph and fluoroscopic images. The measurement errors of the methods were evaluated based on a human cadaveric knee at 11 flexion positions.

**Results:** The accuracy of the WEMS method was determined experimentally to be less than 0.77 mm for the in-plane translations, 3.06 mm for out-of-plane translation, and 1.13° for all rotations, which is better than that of the PI and GD methods.

**Conclusions:** A new volumetric model-based 2D to 3D registration method has been developed for measuring 3D *in vivo* kinematics of natural knee joints with single-plane fluoroscopy. With the equipment used in the current study, the accuracy of the WEMS method is considered acceptable for the measurement of the 3D kinematics of the natural knee in clinical applications. © *2010 American Association of Physicists in Medicine*. [DOI: 10.1118/1.3301596]

Key words: knee kinematics, 2D to 3D registration, x-ray fluoroscopy, genetic algorithm

## I. INTRODUCTION

Knowledge of the three-dimensional (3D) kinematics of the knee joint during activities is essential for understanding the normal function of the joint[1] and the diagnosis of pathology, such as ligament injury and osteoarthritis,[2] and the evaluation of subsequent treatment, including surgery,[3] rehabilitation,[4] and the design of joint replacements.[5] Measurement of knee kinematics is also an important component of biomechanical studies of the musculoskeletal system.[6] Therefore, an accurate method for joint kinematics measurement is needed.

Several techniques are available for the measurement of 3D knee kinematics, but few allow noninvasive measurement with submillimeter accuracy. Imaging methods such as magnetic resonance imaging (MRI) and computed tomography (CT) may be used to provide 3D geometry and poses of knee, but they are limited to static and non-weight-bearing conditions. Skin marker-based methods, including stereophotogrammetry and electromagnetic tracking systems, have been widely used in clinical settings for the measurement of the 3D kinematics of the human body during functional activities.[7–10] However, skin movement artifacts are difficult to prevent without the use of invasive bone pins.[11] The use of intracortical bone pins may not only expose the subjects to risks of infection but may also alter their kinematics. Although mathematical methods have successfully reduced the effects of skin movement artifacts in estimating bone positions,[12] the measurement errors are still too large for an accurate description of the surface kinematics of the articular surfaces, i.e., rolling and sliding motions between surfaces.

Radiographic techniques provide the most direct way to measure joint motions without disturbances caused by soft-tissue artifacts. Surface model-based methods using dynamic fluoroscopy systems have been proposed for the accurate estimation of the 3D poses (positions and orientations) of knee prosthesis components.[13–17] All these approaches work by registering the known 3D CAD surface models of the prosthesis component to the dynamic fluoroscopic images. The

surface model of a prosthesis component is projected onto the fluoroscopic image plane, and the pose of the component is then determined as the 3D pose of the component model that gives the best correspondence between the fluoroscopic image and the projected contours and/or areas of the model component. These methods have been shown to have high accuracy because the metallic components have precisely known geometric features and produce sharp edges in fluoroscopic images. According to Banks and Hodge,[16] the precision values of total knee replacement (TKR) measurement were 0.21 mm, 3.9 mm, and 1.3° for the magnitude of in-plane, out-of-plane, and all rotations error, respectively. Improvements and clinical applications of this type of method have been reported over the past decade.[5,14,18,19] The method has also been assumed to be applicable to natural knee joints[13] even though bones differ fundamentally from TKR components in their form and internal structure. Fluoroscopic images of bones look completely different compared to those of TKR components and have edges that are less well-defined. Bone edge attenuation has been suggested to be the primary factor limiting the theoretical accuracy of this type of method in measuring bone poses with single-plane fluoroscopy.[20] Under real life conditions, the accuracy would likely be worse. However, no well-documented experimental evaluation of these surface model-based methods for measuring natural knee kinematics exists.

Given the limitations in the accuracy of the existing surface model-based methods with single-plane fluoroscopy for the measurement of the kinematics of natural knees, methods using biplanar fluoroscopy[21,22] have been proposed. Although more accurate than single-plane fluoroscopy, biplanar fluoroscopy methods inevitably increase radiation doses, unacceptably constrain the motion of the patient,[14] and sometimes require surgical implantation of metal beads,[22] restricting their use to certain limited populations. These limitations also apply to approaches using multiviews of radiographs for bone pose reconstruction.[23]

More recently, slice-to-volume (SV) registration methods[24] have been developed for accurate intraoperative positioning of the body parts and the surgical instruments using either CT fluoroscopy or cine MRI. Theoretically, these methods can be further developed for the measurement of knee kinematics. However, CT fluoroscopy imaging is too slow for functional joint kinematics and the rotating C-arm also limits the imaging of the knee joint during weight-bearing functional activities. Fast cine MRI has been used to provide fast data of a single slice of the body parts for SV registration in image-assisted biopsies, interventional therapy of prostate cancer,[25] brain functional MRI,[26] postmortem pathology studies,[27] and anatomical modeling.[28] Piecewise SV registration of MRI slices with segmented parts of a joint could be used for *in vivo* analysis of joint motion. However, since bones of a joint may move out of the imaging slice in most functional activities, the application of MR slice-volume registration will be limited in the study of functional weight-bearing activities such as level walking. Another limitation of an MR-based method is that integrated measurements with devices including metal components and wire, for example, force plates, is not possible.

From the above review, it appears that a single-plane fluoroscopy method with high accuracy in measuring the *in vivo* 3D bone kinematics will contribute significantly to relevant clinical studies and applications. However, the accuracy of such a method must be established before application. The accuracy of the measurement of the 3D natural knee kinematics using single-plane fluoroscopy has been reported,[29,30] but few reports have clearly documented the technical aspects of the methods and the experimental procedures in determining the accuracy, as these studies were mainly reporting the results of the application of the methods.[29,30] All these studies used methods similar to those for total knee replacements, but with the surface models of the bones of the normal knee generated from CT images. From these studies, the measurements for all axes of rotation and translation were accurate, but translation along the projection axis had much less accuracy mainly because the projection image of the surface models is much less sensitive to this out-of-plane translation than the in-plane translations. This is a major limitation in the study of the surface kinematics of the knee, such as contact point movements, because the motion of a point on the bone is determined not only by rotations and translations along the axes in the imaging plane but also by those along the projection axis. Komistek *et al.*[29] had to disregard the measured translation of the contact point along the projection axis. Since surface models provide information only on the external structure of the bones, a possible means of improving the out-of-plane accuracy of single-plane fluoroscopy methods may be to include more detailed representations of the internal architecture of the bone models.[29,30]

A method of allowing information from CT images to be used in the 2D to 3D registration process is to register directly the CT volumetric data to fluoroscopic images. Registration of intraoperative fluoroscopic images with preoperative 3D CT images has been used in image-guided surgery.[31] Lemieux *et al.*[32] proposed a registration method based on the comparison of biplanar radiographs and digitally reconstructed radiographs (DRRs) obtained from the CT data. Subsequent developments have led to DRR-based registration methods for aligning single-plane fluoroscopic images and CT scans for image-guided surgery.[33–35] Penney *et al.*[34] compared the performances of six similarity measures for 2D to 3D registration of CT images and single fluoroscopic images. They showed that pattern intensity (PI) and gradient difference (GD) measures were superior to the other measures. In that study, a cadaveric lumbar spine was used for validation and the registration was performed for the whole spine as a rigid body. This is different from requirements for the study of joint kinematics in which each bone should be considered separately. In a later study, Penney *et al.*[35] improved their method of registering one vertebra at a time. However, their method gave an out-of-plane translation error of 7.2 mm, which is still too great a difference for an accurate description of the knee joint kinematics. Direct evaluation of the accuracy of PI and GD on knee kinematics is needed. Registration using PI and GD relies on gray scales

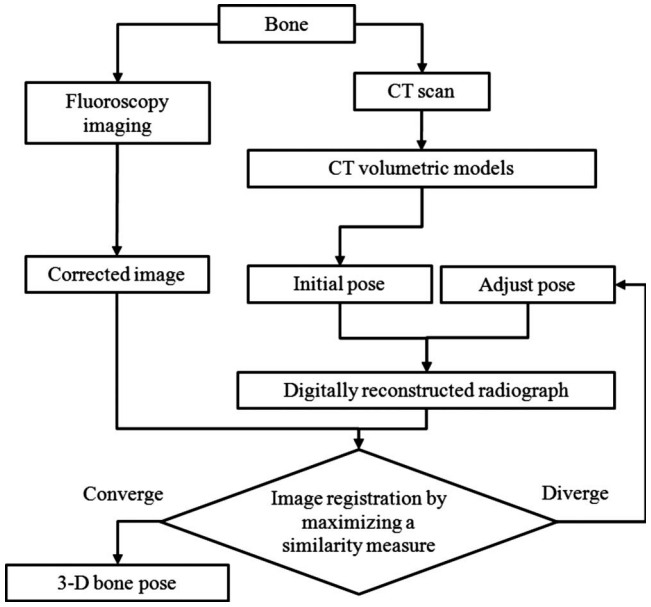


FIG. 1. The general procedure of the new registration method.

and strong gradients associated with prominent bony features. Any noise that can contaminate the grayscales and gradients of the images of the bones, and thus the PI and GD, will affect the registration accuracy. For example, nonuniform fluoroscopy intensity (e.g., owing to the x-ray tube anode heel effect) and the surrounding soft tissues are two such sources of noise during measurements. Thus, a similarity measure that takes into account the noise from these sources may produce a more accurate registration outcome.

The purposes of the study were to develop a new volumetric model-based 2D to 3D registration method with a new similarity measure for measuring natural knee kinematics with single-plane fluoroscopy that takes into account of the noise from the abovementioned sources, to determine experimentally the measurement errors, and to compare the performance between PI, GD, and our new measure.

## II. THE NEW VOLUMETRIC MODEL-BASED REGISTRATION METHOD

### II.A. Overview

The general procedure for the proposed volumetric model-based CT-to-fluoroscopy image registration method is shown in Fig. 1. The CT data of a joint are used to create volumetric computer models for each of the bones. Fluoroscopic images of the same joint under static conditions or during dynamic motion are also obtained. The 3D pose of the bone in each fluoroscopic image frame is then obtained by using an optimization procedure to search for the pose of the bone model whose DRR best matches the fluoroscopic image according to a similarity measure called the weighted edge-matching score (WEMS). The registered poses of the bones for all image frames can then be used to obtain the 3D kinematics of the joint. A more detailed description of the method is given below.

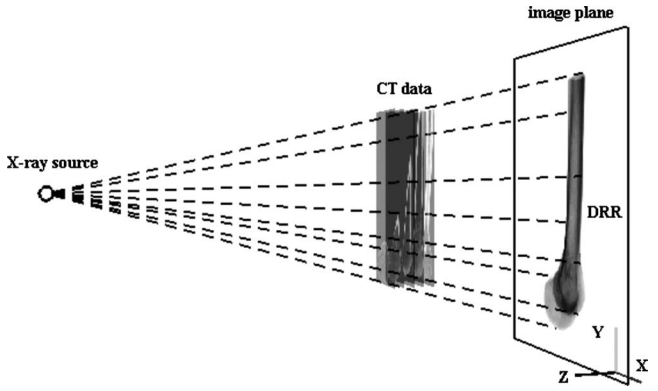


FIG. 2. Perspective projection model of the fluoroscopy system. *X* and *Y* axes define the image plane. Rays of the point source x-ray passing through the CT volume are projected onto the image plane to form a DRR.

### II.B. Bone model creation

The bones of the joint under study are scanned by CT. The CT data for each bone segment are then isolated from the original data set by applying a 3D region-growing method. The segmented volume is then checked manually slice-by-slice to ensure that the bony details are completely included in the volume with minimal remaining external soft tissues. In other words, no part of the bone generating gray-value edges and boundaries in the DRR is missing. Since the influence of the remaining external soft tissues on the DRR is negligible, it is considered that the current segmentation process will not affect the results of the subsequent registration with fluoroscopic images.[33] Bones with negligible relative motions, such as the tibia and fibula, may be considered as a single component during the registration procedure to improve the accuracy of the measurement.

### II.C. Projection model of the fluoroscopy system

The formation of a fluoroscopic image can be modeled as an ideal perspective projection of a point source x-ray onto a planar phosphor screen upon which the image is formed, as shown in Fig. 2. Model parameters, including those for fluoroscopic image distortion and the position of the x-ray source, are obtained through a calibration procedure using a $30\times30$ $cm^2$ transparent calibration box. Two parallel sides of the box are a reseau plate and a star plate that are both marked with lead markers. During calibration, the box is placed with the reseau plate on the image intensifier of the fluoroscopy and its image is obtained. The reseau plate image is used to correct image distortions, such as pincushion distortions and nonuniform scaling, via a modified polynomial method,[36] while that of the star plate is used to estimate the position of the point source x-ray by minimizing the projection errors of the control points on the plate. Given the parameters, a particular fluoroscopy system is modeled and can then be used for the generation of DRRs.

The DRRs are produced by casting rays through the CT volume and projecting them onto the image plane, as shown in Fig. 2. Each of these rays goes through a number of voxels of the CT volume. The Hounsfield numbers of these voxels

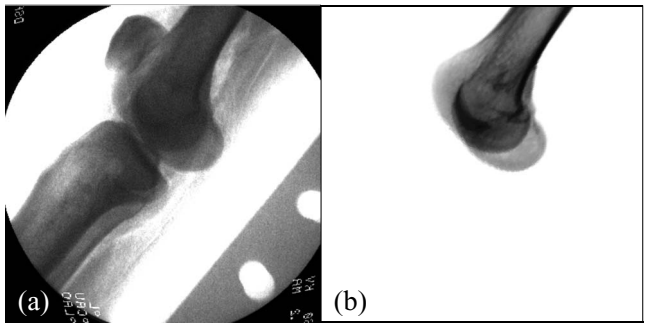


FIG. 3. (a) A fluoroscopic image ($I_{\mathrm{fl}}$) of a knee and (b) a DRR of its femur ($I_{\mathrm{DRR}}$).

are then integrated along the ray and projected onto an imaging plane to obtain a DRR image resembling a radiograph.[34] DRRs are synthetic x-ray images with detailed internal information of the bony structure.

## II.D. Similarity measures

During the search for the 3D pose of a bone model whose DRR image best matches the fluoroscopic image, a similarity measure is necessary to describe the level of similarity between the DRR ($I_{\mathrm{DRR}}$) and the fluoroscopic image ($I_{\mathrm{fl}}$) (Fig. 3). The PI and GD previously proposed in literature[33,35] and the new WEMS are described as follows.

### II.D.1. PI

The pattern intensity measure[33] attempts to subtract the DRR ($I_{\mathrm{DRR}}$) from the fluoroscopic image ($I_{\mathrm{fl}}$) so that in the optimal registration position the structure from the bone will vanish. The measure is described mathematically as a function of a scaling factor $s$ as follows:

$$\mathrm{PI}_{r,\sigma}(s)=\sum_{i,j}\sum_{d^2\le r^2}\frac{\sigma^2}{\sigma^2+(I_{\mathrm{diff}}(i,j)-I_{\mathrm{diff}}(v,w))^2}, \tag{1}$$

where

$$d^2=(i-v)^2+(j-w)^2, \tag{2}$$

$$I_{\mathrm{diff}}=I_{\mathrm{fl}}-sI_{\mathrm{DRR}}. \tag{3}$$

The PI method operates on a single difference image ($I_{\mathrm{diff}}$), which is created by subtracting the DRR from the fluoroscopic image using a suitable scaling factor, $s$ [Eq. (3)]. Pixel values are only compared if the distance ($d$) between the pixels is less than or equal to a radius $r$ [Eq. (2)]. The constant $\sigma$ is used to ensure that the measure remains near its maximum value when small deviations in intensity (such as those caused by noise) occur. As suggested by Penney *et al.*,[34] $\sigma=10$ and $r=3$ are used in the current study. For each new calculation of the similarity measure PI($s$), the optimum scaling factor $s$ is determined by maximizing PI($s$) using a one-dimensional gradient descent-type search strategy.

### II.D.2. GD

For the calculation of the GD according to Penney *et al.*,[34] $I_{\mathrm{fl}}$ and $I_{\mathrm{DRR}}$ are transformed by applying horizontal and vertical Sobel templates to obtain four gradient images, namely, $\partial I_{\mathrm{DRR}}/\partial i$, $\partial I_{\mathrm{DRR}}/\partial j$, $\partial I_{\mathrm{fl}}/\partial i$, and $\partial I_{\mathrm{fl}}/\partial j$. These gradient images represent the partial derivatives of the DRR and those of the fluoroscopic image intensities along the two orthogonal axes of the images. Vertical and horizontal gradient difference images, $I_{\mathrm{diff}\,V}$ and $I_{\mathrm{diff}\,H}$, are then calculated by subtracting the DRR gradient image intensities from the fluoroscopic gradient image intensities as follows:

$$I_{\mathrm{diff}\,V}(i,j)=\frac{\partial I_{\mathrm{fl}}}{\partial i}-s\frac{\partial I_{\mathrm{DRR}}}{\partial i},$$

$$I_{\mathrm{diff}\,H}(i,j)=\frac{\partial I_{\mathrm{fl}}}{\partial j}-s\frac{\partial I_{\mathrm{DRR}}}{\partial j}, \tag{4}$$

where $s$ is a scaling factor and is so chosen that at the optimal registration position, the structure of the bone will vanish. The gradient difference measure is defined as

$$\mathrm{GD}(s)=\sum_{i,j}\frac{A_v}{A_v+(I_{\mathrm{diff}\,V}(i,j))^2}+\sum_{i,j}\frac{A_h}{A_h+(I_{\mathrm{diff}\,H}(i,j))^2}, \tag{5}$$

where $A_v$ and $A_h$ are constants that are set to the variance of the pixel intensities in the respective (vertical and horizontal) gradient fluoroscopic image. By using both vertical and horizontal gradient images, the similarity measure is able to compare the directions of the gradients as well as their magnitudes.

### II.D.3. WEMS

For the calculation of the WEMS, the Canny method[37] is first used to obtain edge images $E_{\mathrm{fl}}$ and $E_{\mathrm{DRR}}$ for $I_{\mathrm{fl}}$ and $I_{\mathrm{DRR}}$, respectively (Fig. 4). The Canny method uses a high and a low threshold to detect strong and weak edges and includes the weak edges in the output only if they are connected to strong edges. This makes it less likely to be fooled by noise and more likely to detect true weak edges, which is different from other edge-detection methods. After edge detection, $E_{\mathrm{fl}}$ is then dilated to become a dilated edge image $A_1$ by applying a $3\times3$ cross-shaped structuring element $M$ to each pixel of the edges once, where

$$M=\begin{bmatrix}0&1&0\\1&1&1\\0&1&0\end{bmatrix}, \tag{6}$$

$$A_1=A_0\oplus M=\mathrm{dilate}(A_0,M), \tag{7}$$

$$A_0=E_{\mathrm{fl}}. \tag{8}$$

Applying $M$ once again to the dilated image $A_1$ gives a new dilated image $A_2$. Repeating the operation $d$ times will produce d dilated images, i.e., $A_1,A_2,\ldots,A_d$. Summation of these dilated images and $E_{\mathrm{fl}}$ will produce a final dilated edge image $B_{\mathrm{fl}}$ with a dilation band of $(2d+1)$ pixels in width [Fig. 4(c)] as follows:

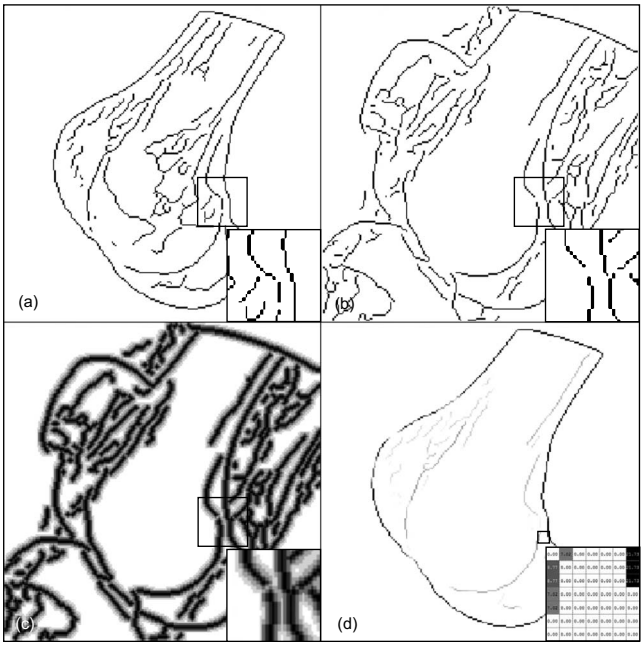


FIG. 4. Image processing steps for WEMS. (a) Edge image of the DRR in Fig. 3(b): $E_{\mathrm{DRR}}$. (b) Edge image of the fluoroscopic image in Fig. 3(a): $E_{\mathrm{fl}}$. (c) $B_{\mathrm{fl}}$ obtained by dilation of $E_{\mathrm{fl}}$ with a small band. (d) Edge image ($E_{\mathrm{reg}}$), which is formed by the overlapping edges of $B_{\mathrm{fl}}$ and $L_{\mathrm{DRR}}$. The inlet figures in (a), (c), and (d) show the detailed images of the marked areas. See main text for detailed definitions of the symbols.

$$B_{\mathrm{fl}} = \frac{1}{d+1}\sum_{i=0}^{d} A_i, \quad A_{n+1} = A_n \oplus M. \tag{9}$$

In order to maintain the values of the pixels in the original edge to unity, the dilated image $B_{\mathrm{fl}}$ is divided by $(d+1)$. In $B_{\mathrm{fl}}$, the value of each pixel in the band, i.e., pixels within a distance $(d)$ to the original edge, is set to be inversely proportional to its shortest distance from the original edge. In the current study, $d=3$ was chosen empirically. The use of a dilated edge image enables the DRR edges within the band to be considered in the WEMS value, which improves the convergence.

Similar to manual registration, long edges are given greater weightings in the similarity score. The weightings are determined based on $E_{\mathrm{DRR}}$. The longer the edge to which 1 pixel belongs, the greater the weighting of the pixel. In order to determine the weightings, the 8-connected length of each edge in terms of the number of pixels is calculated first. That is, two pixels adjacent to each other vertically, horizontally or diagonally are considered to be on the same edge. The 8-connected length of each edge to the $p$th power is then stored in each of the corresponding pixels in $L_{\mathrm{DRR}}$ that has the same size as $E_{\mathrm{DRR}}$. In the current study, $p$ was selected as 0.5 based on a systematic search using computer simulations. This weighting method is designed to give longer edges higher weightings, while maintaining the weightings within a reasonable range. Each pixel of the dilated image $B_{\mathrm{fl}}$ is then multiplied by the value of the corresponding pixel of $L_{\mathrm{DRR}}$ to produce image $E_{\mathrm{reg}}$ [Fig. 4(d)] as follows:

$$E_{\mathrm{reg}}(x,y) = L_{\mathrm{DRR}}(x,y) B_{\mathrm{fl}}(x,y). \tag{10}$$

That is, the resulting $E_{\mathrm{reg}}$ is formed by the overlapping edges of $L_{\mathrm{DRR}}$ and $B_{\mathrm{fl}}$, and the value of a pixel in $E_{\mathrm{reg}}$ provides a measure of the distance of the corresponding pixel in $E_{\mathrm{DRR}}$ from the nearest pixel in the overlapped $E_{\mathrm{fl}}$. The smaller the value, the greater the distance. WEMS is then defined as the total area of $E_{\mathrm{reg}}$ as a percentage of the total area of $L_{\mathrm{DRR}}$ as follows:

$$\mathrm{WEMS}_{d,p} = \frac{\Sigma_{(x,y)} E_{\mathrm{reg}}(x,y)}{\Sigma_{(x,y)} L_{\mathrm{DRR}}(x,y)}. \tag{11}$$

The WEMS value ranges from 0 to 1. The greater the WEMS value, the closer $E_{\mathrm{DRR}}$ is matched with $E_{\mathrm{fl}}$ because there is a greater percentage of matched weighted edges in $L_{\mathrm{DRR}}$. A WEMS value of 0 indicates that no edges are matched, whereas the maximum WEMS value of 1 indicates that all edges are matched.

### II.E. Optimization

For the search of a model pose such that its DRR best matches, the measured fluoroscopic image, an optimization procedure is used. The three translations and three rotations of the bone model are taken as the design variables, and the optimization problem is to find the optimum design that minimizes $-\mathrm{PI}(s)$, $-\mathrm{GD}(s)$ or $-\mathrm{WEMS}_{d,p}$ [Eqs. (1), (5), and (11), respectively]. Since the feasible region of the problem is nonlinear, the genetic algorithm (GA) is chosen to find the global minimum.[38] The GA is a zero-order optimization algorithm and has been shown to be robust in searching for the global optimum.[39] The initial guess of the design variables is obtained through a manual positioning procedure using a graphical user interface (GUI) program described in Sec. II F. Given the initial guess, an initial population of a size of 50 for the GA is then randomly created within a range of 30 and 100 mm for in-plane and out-of-plane translation, and 20° for all rotations. The maximum number of generations is 100. The current optimization parameters are determined based on computer simulations, considering both convergence rate and optimum results. A further increase in the number of generations and population size may slightly improve the optimum design, but the time required for convergence will increase excessively.

### II.F. GUI program

The GUI program was developed using MATLAB (The Mathworks, Inc., USA), which allows the user to construct a virtual fluoroscopy system using system parameters obtained from the experimental system calibration. The program also allows the user to visualize the corrected fluoroscopic images and the CT-derived computer bone models. In the virtual world, the view point is set to the x-ray focus position, which allows the user to visualize the projected bone model on top of the fluoroscopic image. With this arrangement, and through convenient mouse control of the bone pose, the user can quickly find an initial pose of the model for the subsequent registration using optimization. This process is re-

peated for all the bones of the joint. After registration of the bones for a series of image frames, the 3D motion of the bones can be viewed from any view point.

## III. EVALUATION OF ACCURACY

The accuracy of the WEMS method for the kinematics of the knee was evaluated and compared to that obtained with the PI and GD methods, both theoretically using computer simulation and experimentally with an *in vitro* approach. The former determines the theoretical accuracy of the method, while the latter gives the accuracy in realistic situations. All the analyses were performed on a notebook computer with an Intel Core 2 Duo T7300 CPU and 3 Gbytes of RAM.

### III.A. Computer simulation

Computer simulation allows the evaluation of registration methods without the presence of noise that can contaminate the images of the bones and thus affect the registration accuracy. This noise includes the fluoroscopic image distortion, nonuniform fluoroscopy intensity, and effects of the surrounding soft tissues.

The computer simulation was performed using CT bone models of a cadaveric knee, namely, the femur, tibia, and fibula, within a projection model of the fluoroscopy system used in the *in vitro* experiment to be described in Sec. III B. The focal length from the x-ray source to the center of the image plane was 1260 mm. The image plane was a circular plate with a diameter of 300 mm. The CT model of the knee was first placed at a known (true) pose in the middle of the imaging space, and the DRR of the CT model was generated to give a simulated fluoroscopic image with a size of $1020 \times 932$ pixels. Thirty different poses of the knee in the imaging space were then created by adding random deviations to each degree of freedom of the original pose of the knee while the tibia remained stationary. The ranges of the random deviations were 10 mm for all translations, 145° for flexion, and 25° for abduction/adduction and internal/external rotations.[40] Thirty simulated fluoroscopic images corresponding to the 30 poses were also generated. The PI, GD, and WEMS methods were then used to register each of the bone models to each of the simulated fluoroscopic images using the previously described optimization procedure with the same initial guess obtained through a quick manual positioning. The registration errors were then calculated for each of the methods.

### III.B. Experimental evaluation

#### *III.B.1. Experimental procedure*

An *in vitro* experiment was performed to evaluate the measurement errors of the PI, GD, and WEMS methods using a fresh-frozen intact normal left knee, a fluoroscopy system (Angiography, Advantx LCA, GE, France), a motion capture system (Vicon, Oxford Metrics, UK), and a CT system (CT, PQ-5000, Picker International, USA). The knee specimen had a length of 25 cm proximal to the joint line and 25 cm distal. The proximal femur and the distal tibia were fixed with bone cement on a plastic frame made of acrylonitrile butadiene styrene plastic, which is highly rigid (Fig. 5). The plastic frame was built to allow flexion of the knee at 11 different angles up to 100° at 10° intervals and to ensure that at each flexion position, the bones were fixed relative to each other and to the frame. In order to track the poses of the bones and the frame relative to the laboratory coordinate system, two clusters, each with four infrared retroreflective markers, were attached to both the proximal femur and the distal tibia, and eight additional markers were placed on the frame (Fig. 5).

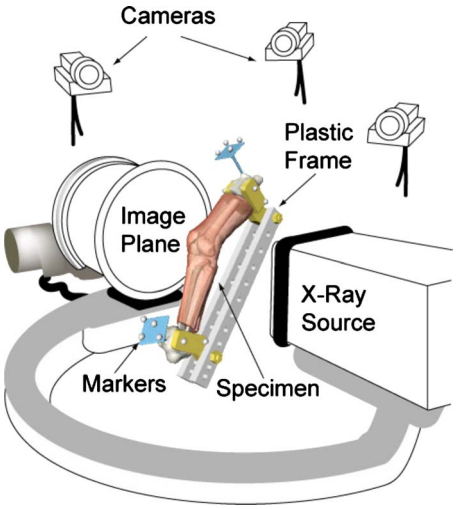


FIG. 5. Setup of the experiment with the specimen fixed on the plastic frame at about 20° of flexion.

At each of the 11 flexion positions defined by the fixation frame, the knee specimen was imaged by CT and fluoroscopy separately. The CT data had $512 \times 512 \times 600$ voxels, each with a size of $0.78125 \times 0.78125 \times 1$ mm$^3$. With the CT data, the spatial relationships of the femur, tibia, and the infrared retroreflective markers were accurately determined. During fluoroscopic imaging, the positions of the retroreflective markers on the specimen/fixation frame construct were also measured using the Vicon system. For each flexion position, 20 trials of simultaneous fluoroscopic imaging and Vicon measurements were performed. The CT data at the extended position were used to create the bone models as described in Sec. II B and to define the local coordinate systems for the femur and tibia, which were chosen to be parallel to the CT coordinate system but with origins at the centroid of each bone. The pose of the bone in space was described in terms of homogeneous transformation matrices that are functions of the three translations and the three rotations. Homogeneous transformation matrices for the femur and tibia were defined with respect to the CT coordinate system, namely, ${}^{CT}T_f$ and ${}^{CT}T_t$, respectively. It is noted that other flexion positions can also be used for bone model creation, as a model of a bone is independent of its position relative to other bones. With the bone models, poses of the femur relative to the tibia under the CT coordinate system, ${}^{f}T_t$, at each flexion angle were then determined by minimizing the root mean squared distance between the points of

TABLE I. Means (standard deviations) of the errors of the bone and knee poses estimated using the PI, GD, and WEMS methods, and corresponding run time over 30 computer simulated trials. Directions are with respect to the fluoroscopic coordinate system, where $X$ and $Y$ are parallel to the image plane and $Z$ is perpendicular to the image plane.

| | WEMS | | | GD | | | PI | | |
|---|---|---|---|---|---|---|---|---|---|
| | Femur | Tibia | Knee | Femur | Tibia | Knee | Femur | Tibia | Knee |
| $X$ (mm) | 0.00 (0.10) | 0.09 (0.15) | 0.12 (0.24) | −0.08 (0.10) | 0.08 (0.11) | −0.15 (0.20) | −0.07 (0.12) | −0.12 (0.16) | 0.15 (0.25) |
| $Y$ (mm) | 0.00 (0.06) | 0.04 (0.21) | −0.02 (0.16) | −0.05 (0.14) | 0.05 (0.15) | 0.06 (0.14) | 0.06 (0.16) | −0.04 (0.22) | 0.03 (0.26) |
| $Z$ (mm) | −0.26 (1.32) | 0.21 (1.73) | 0.20 (1.95) | −0.73 (1.86) | −0.61 (1.93) | 0.26 (2.88) | −0.68 (1.90) | 0.44 (2.11) | 0.86 (3.12) |
| $\theta_x$ (deg) | 0.03 (0.22) | 0.02 (0.29) | 0.10 (0.40) | −0.04 (0.48) | 0.04 (0.51) | −0.11 (0.50) | 0.02 (0.46) | 0.05 (0.61) | 0.12 (0.86) |
| $\theta_y$ (deg) | −0.15 (0.23) | −0.13 (0.30) | −0.03 (0.42) | −0.28 (0.40) | −0.29 (0.43) | −0.02 (0.68) | −0.26 (0.32) | −0.22 (0.53) | −0.31 (0.70) |
| $\theta_z$ (deg) | −0.03 (0.15) | 0.01 (0.32) | 0.11 (0.41) | 0.07 (0.14) | 0.05 (0.14) | 0.04 (0.38) | 0.05 (0.21) | 0.07 (0.35) | 0.16 (0.49) |
| Run time (s) | 277 (50) | 266 (65) | | 338 (64) | 354 (74) | | 289 (44) | 329 (67) | |

each model surface to the closest points on the corresponding bone model at the extended position using the iterative closest point algorithm[41] to obtain ${}^{CT}T'_f$ and ${}^{CT}T'_t$ at each flexion position. These were taken as the "true" poses of the knee joint at that flexion angle. The root mean squared errors of the distances between corresponding points of the bone models reconstructed from a different CT data set at each flexion angle were all less than 0.025 mm. The true bone poses relative to the laboratory coordinate system were then determined using the positions of the markers of the clusters captured by the Vicon system. The variance of the repeated measurements of the positions of a single static marker by the Vicon system was determined to be less than 0.12 mm. The fluoroscopy system and motion capture system were integrated through simultaneous measurement of the accurately positioned lead markers and five infrared retroreflective markers on the calibration box to enable the description of the bone poses relative to the same coordinate system, obtained either by the Vicon system or by the 3D registration procedure.

#### III.B.2. Convergence test

The robustness of the WEMS method was evaluated by a convergence test using a fluoroscopic image of the extended cadaveric knee. For each femur and tibia, 30 initial guesses of the pose of the bone were created by adding random deviations to each degree of freedom of the true pose of the bone. The translation of the bone was 8 mm with a random direction in the image plane, i.e., the $X$-$Y$ plane, and either 40 or −40 mm along the out-of-plane direction, i.e., the $Z$ axis. The deviation in rotation was 8° along a random axis of rotation. For each initial guess, the errors of the registered poses of the bones and the knee were obtained for subsequent statistical analysis.

#### III.B.3. Registration with PI, GD, and WEMS

For each of the 220 experimental trials, the bone models were registered to the fluoroscopic image one by one using each of the PI, GD, and WEMS methods with the same initial guess obtained through a quick manual positioning. The registration errors were then calculated for each of the methods.

### III.C. Statistical analysis

For the computer simulation, the means and standard deviations of the errors in the poses of the bones and knee across the 30 simulated trials were calculated for each method, i.e., PI, GD, and WEMS, to determine the theoretical accuracy of the methods. For the experimental tests, the errors in the poses of the bones and knee were ensemble averaged over the 220 trials of the 11 flexion positions for PI, GD, and WEMS, respectively. The mean values indicate the bias of the method, while the standard deviations indicate the precision. For convergence test, the means and standard deviations of the errors of the 30 initial guesses were calculated to determine the robustness of the WEMS method. For the computer simulation and experimental tests, the means and standard deviations of the time required for registrations were also calculated.

## IV. RESULTS

### IV.A. Computer simulation

Computer simulation results showed that the errors in the poses of the knee and its bones were comparable for all methods, with those of the WEMS method being slightly lower (Table I). For the WEMS method, the magnitudes of the means (standard deviations) for the femoral pose errors were less than 0.004 (0.10) mm for the in-plane translation components ($X$ and $Y$), 0.26 (1.32) mm for the out-of-plane translation ($Z$), and 0.15° (0.23°) for all the angular components. The corresponding values for the GD method were 0.08 (0.14) mm, 0.73 (1.86) mm, and 0.28° (0.48°), respectively. For the PI method, they were 0.07 (0.16) mm, 0.68 (1.90) mm, and 0.26° (0.46°), respectively. Tibial pose errors were slightly greater than those of the femur for all three methods (Table I).

For knee poses, the WEMS method gave the magnitudes of the means (standard deviations) of less than 0.12 (0.24) mm for the in-plane translation components, 0.20 (1.95) mm for the out-of-plane translation, and 0.11° (0.42°) for all the angular components. The corresponding values for the GD method were 0.15 (0.20) mm, 0.26 (2.88) mm, and 0.11° (0.68°), respectively (Table I). For the PI method, they were 0.15 (0.26) mm, 0.86 (3.12) mm, and 0.31° (0.86°), respec-

TABLE II. The means (standard deviations) of the errors of the bone and knee poses estimated using the PI, GD, and WEMS methods over 220 experimental trials. Directions are with respect to the fluoroscopic coordinate system, where $X$ and $Y$ are parallel to the image plane and $Z$ is perpendicular to the image plane.

| | WEMS | | | GD | | | PI | | |
|---|---|---|---|---|---|---|---|---|---|
| | Femur | Tibia | Knee | Femur | Tibia | Knee | Femur | Tibia | Knee |
| $X$ (mm) | −0.42 (0.56) | −0.34 (0.86) | 0.24 (0.77) | −0.34 (0.72) | −0.77 (1.32) | −0.60 (0.71) | −1.01 (1.38) | −0.85 (1.63) | 0.83 (0.76) |
| $Y$ (mm) | 0.68 (0.72) | −0.24 (0.61) | 0.04 (0.75) | 0.55 (0.87) | −0.46 (0.85) | −0.31 (0.86) | 0.66 (1.16) | −0.44 (0.94) | −0.59 (0.98) |
| $Z$ (mm) | −0.94 (3.23) | −0.38 (4.61) | 0.41 (3.06) | 1.64 (3.70) | −2.83 (6.03) | −3.12 (6.02) | 3.37 (5.17) | 6.28 (7.39) | 11.39 (8.55) |
| $\theta_x$ (deg) | −0.52 (0.77) | 0.38 (0.57) | 0.51 (0.73) | 0.44 (0.70) | −0.42 (0.93) | −0.61 (1.26) | −0.02 (0.99) | −0.50 (1.08) | 0.58 (1.84) |
| $\theta_y$ (deg) | 0.91 (0.83) | 0.13 (1.21) | 0.59 (1.10) | −0.35 (0.92) | 0.10 (0.71) | −0.83 (1.60) | −0.43 (0.96) | 0.60 (1.33) | −0.61 (2.05) |
| $\theta_z$ (deg) | 0.55 (0.75) | −0.81 (0.49) | −0.40 (1.13) | −0.46 (0.72) | −0.50 (0.68) | 0.04 (0.76) | 0.65 (0.51) | −0.31 (0.81) | 0.60 (0.36) |
| Run time (s) | 280 (42) | 259 (74) | | 331 (92) | 363 (83) | | 295 (52) | 325 (68) | |

tively (Table I). When comparing all three methods, the run time of the GD method took the longest, while the WEMS method was the fastest, both for the femur and for the tibia registration (Table I).

### IV.B. Experimental evaluation

Experimental results showed that the errors of the global poses of the bones using the WEMS method were generally smaller than those from the PI and GD methods. The WEMS method had means (standard deviations) of the absolute tibial pose errors of less than 0.34 (0.86) mm, 0.38 (4.61) mm, and 0.81° (1.21°) for the in-plane translation components, out-of-plane translation component, and all angular components, respectively. The corresponding values for the GD method were 0.77 (1.32) mm, 2.83 (6.03) mm, and 0.50° (0.93°), and those for the PI were 0.85 (1.63) mm, 6.28 (7.39) mm, and 0.60° (1.33°) (Table II). For the femur, the WEMS method had means (standard deviations) of the absolute tibial pose errors of less than 0.68 (0.72) mm, 0.94 (3.23) mm, and 0.91° (0.83°) for the in-plane translation components, out-of-plane translation component, and all angular components, respectively. The corresponding values for the GD method were less than 0.55 (0.87) mm, 1.64 (3.70) mm, and 0.46° (0.92°), and those of the PI were 1.01 (1.38) mm, 3.37 (5.17) mm and 0.65° (0.99°) (Table II). Again, the run time of the GD method was the longest, while that of the WEMS was the shortest, both for the femur and for the tibia (Table II). For a better understanding of the differences between the two methods in the measurement errors, especially the out-of-plane translation, cost function values for both the femur and tibia as a function of the out-of-plane translation for these three methods were generated for all test positions and a typical case is given in Fig. 9.

With the measurement errors of the femur and tibia, the errors of the poses of knee kinematics using the WEMS method were also less than those from the GD method, especially those of the out-of-plane component. The means (standard deviations) of the knee pose errors using the WEMS method were less than 0.24 (0.77) mm, 0.41 (3.06) mm, and 0.59° (1.13°) for the in-plane translation components, out-of-plane translation component, and all the angular components, respectively, while the corresponding values for the GD method were 0.60 (0.86) mm, 3.12 (6.02) mm, and 0.83° (1.60°), and those for the PI were 0.83 (0.98) mm, 11.39 (8.55), and 0.61° (2.05°) (Table II).

### IV.C. Convergence test

In the analysis of the experimental data, the GA optimization procedure successfully converged to an optimum for each of the thirty different initial guesses. Over the generations, when the mean fitness value approaches the best fitness value, a local minimum is reached (Fig. 6, generation 18). The GA was able to escape the local minimum as indicated by the sudden separation of the mean fitness value from the best value in Fig. 6. With this ability, the GA could further reduce the fitness value and finally converge to the final optimum solution. For example, at generation 3 of one of the 30 trials, the current best pose of the femur is still far from the true position, as shown by the mismatch between the femoral model and the underlying fluoroscopic image in Fig. 7(a). As the number of the generation increases, the current best fitness pose of the femur approaches the final

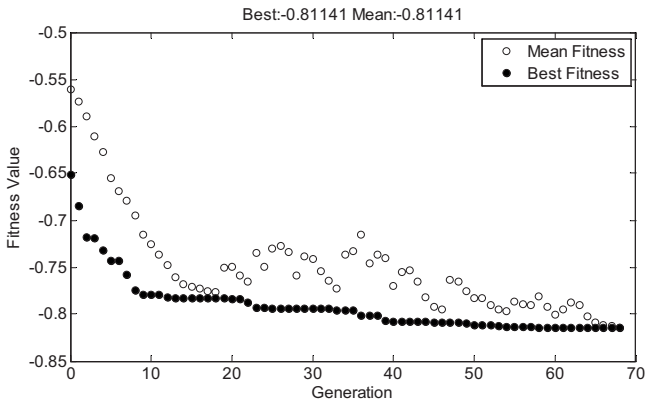


FIG. 6. Fitness values (i.e., negative WEMS values) over generations during the optimization process of the registration of the femur in a typical experimental trial using GA. The best and mean fitness values across all the individuals for each generation are indicated by solid and open circles, respectively. The fitness values decreased with increased generations and finally converged to the final solution.

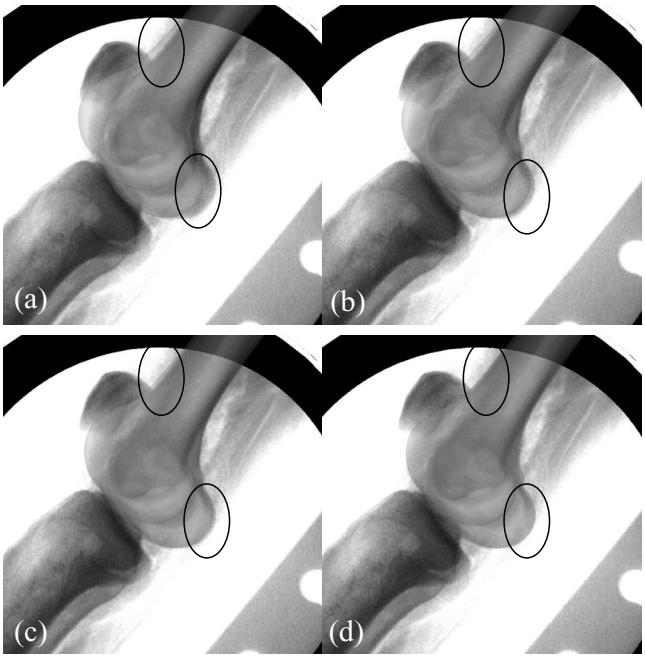


FIG. 7. Best fitted poses of the femur in the same trial as used in Fig. 6 at generation 3 (a), 5 (b), 26 (c) and at the final converged optimum pose (d). The reduction in the differences between the bone and the fluoroscopic image over generations can be seen visually within the marked areas.

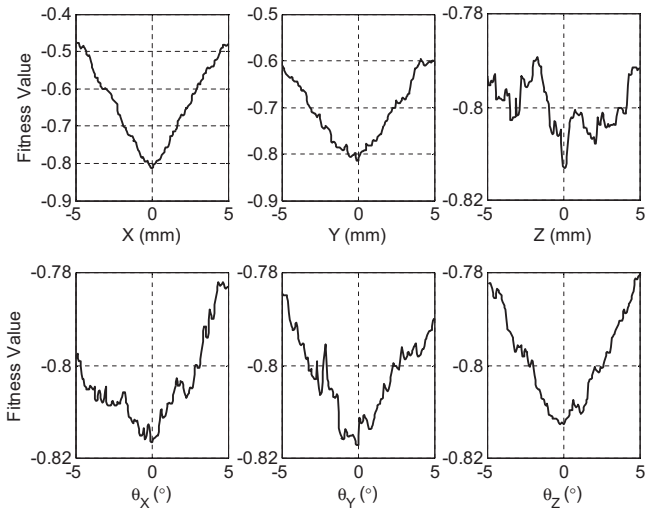


FIG. 8. Changes in the fitness values (i.e., negative WEMS values) for each component of the femoral poses in the neighborhood of 5 mm or 5° around the converged optimum pose while keeping the other components unchanged. The fitness values at the optimum pose are very close to the minimum fitness values. Directions are with respect to the fluoroscopic coordinate system, where *X* and *Y* are parallel to the image plane and *Z* is perpendicular to the image plane.

optimum solution [Figs. 7(b) and 7(c)], which almost exactly covers the area of the femur in the fluoroscopic image [Fig. 7(d)].

Given the nonlinear nature of the registration problem, as shown by the changes in the fitness values of the WEMS measure of the femoral poses in a neighborhood of 5 mm and 5° around the converged optimum pose (Fig. 8), the final optimum poses obtained were not strongly dependent on initial guesses. For the randomly generated 30 initial positions, the magnitudes of the means (standard deviations) of the femoral pose errors were less than 0.31 (0.13) mm, 0.20 (1.31) mm, and 0.55° (0.33°) along the in-plane direction, the out-of-plane direction, and all the angles, respectively. For the tibial pose errors, the magnitudes of the means (standard deviations) were less than 0.42 (0.31) mm, 1.14 (2.06) mm, and 0.26° (0.72°) along the in-plane direction, the out-of-plane direction, and all the angles, respectively. For the knee pose measurements, the magnitudes of the means (standard deviations) of the errors were less than 0.47 (0.50) mm, 1.72 (2.97) mm, and 0.70° (0.83°) along the in-plane direction, the out-of-plane direction, and all the angles, respectively (Table III).

## V. DISCUSSION

A new volumetric model-based 2D to 3D registration method has been developed for measuring 3D *in vivo* kinematics of natural knee joints with single-plane fluoroscopy, taking into account of the influences from tissues other than the targeted bones, and noise from the fluoroscopy system itself. The method was shown experimentally to have measurement errors less than 0.24 (0.77) mm for in-plane translations, 0.41 (3.06) mm for out-of-plane translations, and 0.59° (1.13°) for all rotations, which were smaller than those of the PI and GD methods, two of the best registration methods suggested in literature.[34] The error for the out-of-plane translation by the WEMS is smaller than previously published errors of other bone registration methods.[30,42] Under the same conditions, no obvious failed registrations for all three methods were encountered in our analyses. The error levels of the WEMS method are comparable to the reported errors for TKR registration methods.[14–16] Similar to the TKR registration methods, the WEMS method should be considered acceptable for most clinical applications.

Apart from the definitions of the similarity measures, the accuracy of the bone pose obtained using the current 2D to 3D registration methods is also affected by factors such as resolution of the CT data, pixel size of the fluoroscopic image and the projection geometry of the fluoroscopy system. Because of the different effects from these factors, the accuracy of the registration methods can be higher than the resolution of the CT data of the bone. In the current study, the

TABLE III. Means (standard deviations) of the errors of the WEMS method in the convergence test. Directions are with respect to the fluoroscopic coordinate system, where *X* and *Y* are parallel to the image plane and *Z* is perpendicular to the image plane.

| | Femur | Tibia | Knee |
|---|---|---|---|
| *X* (mm) | −0.17 (0.13) | −0.42 (0.31) | −0.47 (0.50) |
| *Y* (mm) | −0.31 (0.08) | −0.23 (0.25) | −0.12 (0.28) |
| *Z* (mm) | 0.20 (1.31) | −1.14 (2.06) | −1.72 (2.97) |
| $\theta_x$ (deg) | 0.09 (0.25) | −0.17 (0.47) | 0.21 (0.53) |
| $\theta_y$ (deg) | −0.55 (0.33) | −0.16 (0.72) | −0.70 (0.83) |
| $\theta_z$ (deg) | −0.14 (0.22) | 0.26 (0.31) | −0.38 (0.39) |

performance of the three different similarity measures was compared, while the other factors were controlled. As in other previous studies,[42] the errors of the registered poses were expressed statistically in terms of the associated means and standard deviations. The WEMS method had mean values smaller than the CT resolution. Since mean values indicate the bias of the error distribution, they can be much smaller than the CT resolution.[42] The WEMS method also had standard deviations less than the CT resolution, which may be attributed to two reasons. First, the volumetric CT data of a bone were used to represent the bone as an object, with several hundred thousand voxels. The origin of the bone was then defined as the centroid of the bone volume. Thus, the accuracy of the centroid can be higher than the CT resolution. The second reason is the projection geometry of the fluoroscopy system, which gives the fluoroscopic image high sensitivity to the bone pose change in space. With the current resolution of the fluoroscopy system, this projection geometry enables a spatial resolution of the bone pose higher than the CT resolution. It is also noted that if the errors of all tests are close to the CT resolution, the standard deviation can be smaller than the CT resolution.

Previous studies have used "clean" images of objects outside the body[15,19] or synthetic data[42] when evaluating 2D to 3D registration methods. With clean images, both the PI, GD, and WEMS methods give very small errors (Table I), suggesting that the above similarity measures are well defined for the optimization algorithm to reach an optimum solution that is close to the true solution. The resulting errors can be taken as the lower bound of errors for natural knee kinematics measurements under realistic conditions. However, with real life fluoroscopic images that are subject to noise from the fluoroscopy system itself and from tissues other than the targeted bones, the performance of these methods will depend on their ability to reduce the effects of this noise on the similarity measures, that is, whether the optimum design corresponding to the cost function remains unchanged in the presence of errors. The introduction of soft-tissue structures into the phantom image has been shown to cause a large effect on the performance of some similarity measures previously applied to 2D to 3D image registration.[34] Therefore, the performance of these methods should be evaluated based on more realistic experimental data. While experimental evaluations of the accuracy of TKR registration methods have been reported,[14–16] to the best of our knowledge, the current study is the first well-documented experimental assessment of registration methods for measuring natural knee kinematics with single-plane fluoroscopy.

Establishing the ground truth is essential for the experimental evaluation of the performance of different registration methods. Ideally, the ground truth data should be at least as accurate as the method being tested and should be obtained using an independent method other than fluoroscopy. Previous studies have used fiducial markers in x-ray images,[21,22] but this is not an independent method. Other approaches, such as mechanical positioning systems, are difficult to use on bones located within the body. Infrared stereophotogrammetry has also been used to provide an independent means of determining the ground truth data of total knee implants with an accuracy of 0.2893 mm.[14] In the current study, infrared stereophotogrammetry was used to provide the global poses of the bones using markers attached to the bones through cortical pins. The accuracy of a single point determined by the Vicon system was less than 0.1290 mm. The poses of the knee joint, i.e., tibia relative to the femur, were determined by a CT scan. The use of the fixation frame enabled us to take advantage of the high accuracy of both the CT machine and the Vicon system.

The convergence study showed that the WEMS method, combined with the GA, has the ability to overcome various local minima encountered during the search process to obtain consistent results, regardless of where the search began, as long as the initial guesses are within the tested range (Table III). For most daily activities, the tested region in the current study should encompass the movement range of the knee within the time between two consecutive images of the current fluoroscopy system, i.e., 1/30 s. This suggests that the registered pose for one image can be used as the initial guess for the next image, facilitating the autoregistration of the bone poses for the rest of the image series. This feature helps minimize manual involvement in the registration of image series for *in vivo* knee kinematics during test or functional activities.

The difference between the model-generated DRR and the fluoroscopic image is potentially the most important factor that affects the performance of volumetric model-based registration methods. Superimposed on the signals of the targeted bones in a fluoroscopic image is noise from sources such as overlying and underlying soft-tissue structures and bones. Other fluoroscopy-related sources of noise may include nonuniformity of the intensifier response and geometric distortions.[35] Therefore, the accuracy of a registration method depends on its ability to extract the common features of both the DRR and fluoroscopic images and include them in its cost function. Failure to do this will lead to incorrect cost functions giving wrong optimum solutions. As shown in Fig. 9, the greater errors with the GD method appear to be a result of errors in the cost function curve owing to noise in the fluoroscopic image and not necessarily the failure of the optimization method in reaching a global minimum. The effect of noise in the PI and GD methods was more pronounced in the case of the tibia, with translation errors of 7.4 and 6.7 mm, respectively, in the out-of-plane direction (Fig. 9). The differences between the cost function curves of the femur and tibia suggest that the PI and GD methods are sensitive to the targeted bone as, with different gray values, shape, and structure, the contrast between the bone and the surrounding tissues in the fluoroscopic image may be different. The new registration method improved the accuracy, especially in the out-of-plane translation component, by taking a different approach, namely, WEMS based on the matching of longer edges of the DRR and fluoroscopic edge images. Longer edges seem to be less sensitive to the abovementioned noise and targeted bones so they are more likely to be common features of the DRR and fluoroscopic images. The inclusion of weightings to the edges enabled the optimization

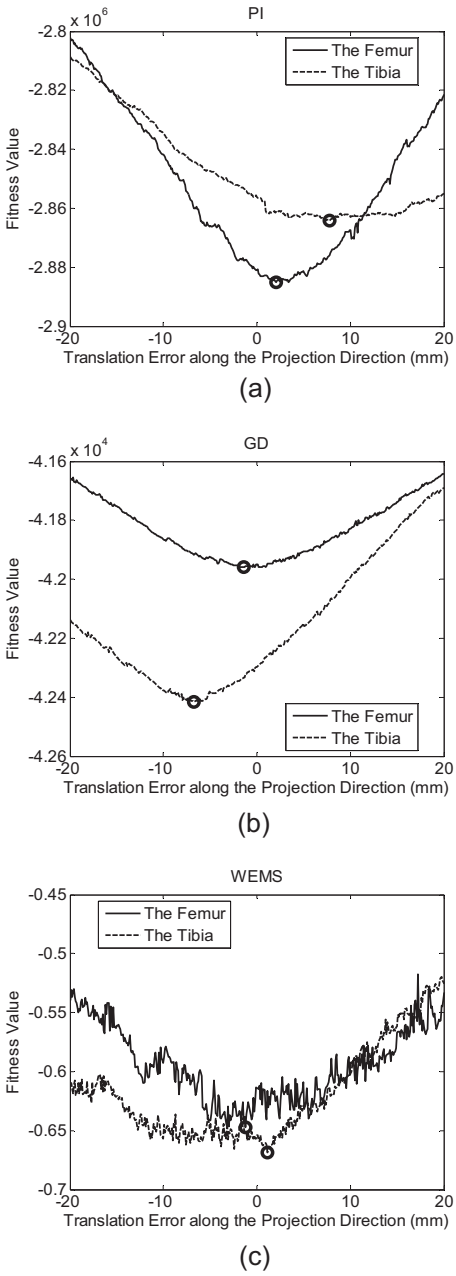


FIG. 9. Fitness values of the femur (solid line) and tibia (dashed line) at positions −20 to +20 mm away from the true poses (i.e., zero error) along the projection axis at an increment of 0.1 mm using the (a) PI, (b) GD, and (c) WEMS methods. The minimum fitness values are marked with circles. It is noted that the minimum values for WEMS occur at poses very close to the true ones.

process to give higher priority to matching long edges, similar to a manual registration process. Numerically, the use of a dilated bandwidth creates slopes on each side of the edge so that the optimization problem is better defined and easier to solve in the bandwidth. With these carefully devised strategies, the WEMS method successfully improves the existing methods in reliably reaching an optimum that is also close to the true solution.

The accuracy of the WEMS method determined in the current study may be further improved if it is used with more advanced fluoroscopy and CT systems that provide higher-quality fluoroscopic images and bone models. More advanced computers or computational techniques, such as parallel distributed computing, will be able to reduce the run time. The method can also be easily combined with biplanar fluoroscopy for higher accuracy. However, the use of a single-plane fluoroscopy system may be preferred as these systems are cheaper and more common in hospitals, and no modification of the hardware is needed to apply the current 2D to 3D registration method for clinical applications. Although there was not much difference in the performance of the WEMS method in registering the femur and tibia compared to the GD method, experimental evaluation of the accuracies is suggested before application to other bones. Compared to SV methods, the current approach adopts high speed single-plane fluoroscopy, which enables the measurement of fast motions within a relatively large space. Incorporating forceplates with the current method will allow for measurements of *in vivo* knee joint kinetics during functional activities.

## VI. CONCLUSIONS

A new volumetric model-based 2D to 3D registration method has been developed for measuring natural knee kinematics with single-plane fluoroscopy. It mimics the manual registration process that gives higher priority to matching of longer edges in the DRR and dilated fluoroscopy images. The accuracy of the WEMS method was determined experimentally to be less than 0.77 mm for the in-plane translations, 3.06 mm for out-of-plane translation, and 1.13° for all rotations, which is better than that of the PI and GD methods. The current study is the first well-documented experimental evaluation study of 2D to 3D registration methods for measuring natural knee kinematics with single-plane fluoroscopy. With the equipment used in the current study, the accuracy of the WEMS method is considered acceptable for the measurement of the 3D kinematics of the natural knee in clinical applications.

## ACKNOWLEDGMENTS

The work presented in this paper was partially supported by the National Science Council of Taiwan (Grant No. NSC-94-2213-E-002-112). The authors are grateful for the assistance of Professor Ming-Jia Jou, Mrs. Jen-Fen Chen, and Dr. Chien-Chung Kuo during the experiment. Thanks go also to the person who donated his body to medical science. The authors (T.-Y.T. and T.-W.L.) contributed equally to this work.

[a]Author to whom correspondence should be addressed. Electronic mail: twlu@ntu.edu.tw; Telephone: +886-2-33653335; Fax: +886-2-33653335.

[1]G. Li, T. W. Rudy, M. Sakane, A. Kanamori, C. B. Ma, and S. L. Woo, "The importance of quadriceps and hamstring muscle loading on knee kinematics and in-situ forces in the ACL," J. Biomech. **32**, 395–400 (1999).

[2]M. R. Maly, P. A. Costigan, and S. J. Olney, "Role of knee kinematics and kinetics on performance and disability in people with medial compartment knee osteoarthritis," Clin. Biomech. (Bristol, Avon) **21**, 1051–1059 (2006).

[3]C. D. Harner, M. A. Janaushek, A. Kanamori, M. Yagi, T. M. Vogrin, and S. L. Woo, "Biomechanical analysis of a double-bundle posterior cruciate ligament reconstruction," Am. J. Sports Med. **28**, 144–151 (2000).
[4]A. D. Georgoulis, A. Papadonikolakis, C. D. Papageorgiou, A. Mitsou, and N. Stergiou, "Three-dimensional tibiofemoral kinematics of the anterior cruciate ligament-deficient and reconstructed knee during walking," Am. J. Sports Med. **31**, 75–79 (2003).
[5]D. A. Dennis, R. D. Komistek, W. A. Hoff, and S. M. Gabriel, "In vivo knee kinematics derived using an inverse perspective technique," Clin. Orthop. Relat. Res. **331**, 107–117 (1996).
[6]T. W. Lu and J. J. O'Connor, "Lines of action and moment arms of the major force-bearing structures crossing the human knee joint: Comparison between theory and experiment," J. Anat. **189**, 575–585 (1996).
[7]T.-W. Lu, H.-C. Lin, and H.-C. Hsu, "Influence of functional bracing on the kinetics of anterior cruciate ligament-injured knees during level walking," Clin. Biomech. (Bristol, Avon) **21**, 517–524 (2006).
[8]H.-L. Chen and T.-W. Lu, "Comparisons of the joint moments between leading and trailing limb in young adults when stepping over obstacles," Gait and Posture **23**, 69–77 (2006).
[9]P. M. Mills, S. Morrison, D. G. Lloyd, and R. S. Barrett, "Repeatability of 3D gait kinematics obtained from an electromagnetic tracking system during treadmill locomotion," J. Biomech. **40**, 1504–1511 (2007).
[10]T.-W. Lu, H.-L. Chen, and S.-C. Chen, "Comparisons of the lower limb kinematics between young and older adults when crossing obstacles of different heights," Gait and Posture **23**, 471–479 (2006).
[11]M. A. Lafortune, P. R. Cavanagh, H. J. Sommer III, and A. Kalenak, "Three-dimensional kinematics of the human knee during walking," J. Biomech. **25**, 347–357 (1992).
[12]T. W. Lu and J. J. O'Connor, "Bone position estimation from skin marker co-ordinates using global optimisation with joint constraints," J. Biomech. **32**, 129–134 (1999).
[13]D. A. Dennis, M. R. Mahfouz, R. D. Komistek, and W. A. Hoff, "In vivo determination of normal and anterior cruciate ligament-deficient knee kinematics," J. Biomech. **38**, 241–253 (2005).
[14]M. R. Mahfouz, W. A. Hoff, R. D. Komistek, and D. A. Dennis, "A robust method for registration of three-dimensional knee implant models to two-dimensional fluoroscopy images," IEEE Trans. Med. Imaging **22**, 1561–1574 (2003).
[15]W. A. Hoff, R. D. Komistek, D. A. Dennis, S. M. Gabriel, and S. A. Walker, "Three-dimensional determination of femoral-tibial contact positions under in vivo conditions using fluoroscopy," Clin. Biomech. (Bristol, Avon) **13**, 455–472 (1998).
[16]S. A. Banks and W. A. Hodge, "Accurate measurement of three-dimensional knee replacement kinematics using single-plane fluoroscopy," IEEE Trans. Biomed. Eng. **43**, 638–649 (1996).
[17]S. Zuffi, A. Leardini, F. Catani, S. Fantozzi, and A. Cappello, "A model-based method for the reconstruction of total knee replacement kinematics," IEEE Trans. Med. Imaging **18**, 981–991 (1999).
[18]D. A. Dennis and R. D. Komistek, "Kinematics of mobile-bearing total knee arthroplasty," Instr Course Lect **54**, 207–220 (2005).
[19]T. Yamazaki, T. Watanabe, Y. Nakajima, K. Sugamoto, T. Tomita, H. Yoshikawa, and S. Tamura, "Improvement of depth position in 2-D/3-D registration of knee implants using single-plane fluoroscopy," IEEE Trans. Med. Imaging **23**, 602–612 (2004).
[20]S. A. Banks, B. J. Fregly, F. Boniforti, C. Reinschmidt, and S. Romagnoli, "Comparing in vivo kinematics of unicondylar and bi-unicondylar knee replacements," Knee Surg. Sports Traumatol. Arthrosc **13**, 551–556 (2005).
[21]B. L. Kaptein, E. R. Valstar, B. C. Stoel, P. M. Rozing, and J. H. C. Reiber, "A new model-based RSA method validated using CAD models and models from reversed engineering," J. Biomech. **36**, 873–882 (2003).
[22]S. Tashman and W. Anderst, "In-vivo measurement of dynamic joint motion using high speed biplane radiography and CT: Application to canine ACL deficiency," J. Biomech. Eng. **125**, 238–245 (2003).
[23]B. Ma, J. Stewart, D. Pichora, R. Ellis, and P. Abolmaesumi, "2D/3D registration of multiple bones," Conference Proceedings of IEEE Engineering in Medicine and Biology Society, 2007, pp. 860–863 (unpublished).
[24]W. Birkfellner, M. Figl, J. Kettenbach, J. Hummel, P. Homolka, R. Schernthaner, T. Nau, and H. Bergmann, "Rigid 2D/3D slice-to-volume registration and its application on fluoroscopic CT images," Med. Phys. **34**, 246 (2007).
[25]B. Fei, J. L. Duerk, D. T. Boll, J. S. Lewin, and D. L. Wilson, "Slice-to-volume registration and its potential application to interventional MRI-guided radio-frequency thermal ablation of prostate cancer," IEEE Trans. Med. Imaging **22**, 515–525 (2003).
[26]B. Kim, J. L. Boes, P. H. Bland, T. L. Chenevert, and C. R. Meyer, "Motion correction in fMRI via registration of individual slices into an anatomical volume," Magn. Reson. Med. **41**, 964–972 (1999).
[27]T. S. Kim, M. Singh, W. Sungkarat, C. Zarow, and H. Chui, "Automatic registration of postmortem brain slices to MRI reference volume," IEEE Trans. Nucl. Sci. **47**, 1607–1613 (2000).
[28]J. Zhengping and P. H. Mowforth, "Mapping between MR brain images and a voxel model," Med. Inf. (Lond) **16**, 183–193 (1991).
[29]R. D. Komistek, D. A. Dennis, and M. Mahfouz, "In vivo fluoroscopic analysis of the normal human knee," Clin. Orthop. Relat. Res. **410**, 69–81 (2003).
[30]I. Kanisawa, A. Z. Banks, S. A. Banks, H. Moriya, and A. Tsuchiya, "Weight-bearing knee kinematics in subjects with two types of anterior cruciate ligament reconstructions," Knee Surg. Sports Traumatol. Arthrosc **11**, 16–22 (2003).
[31]R. Munbodh, D. A. Jaffray, D. J. Moseley, Z. Chen, J. P. S. Knisely, P. Cathier, and J. S. Duncan, "Automated 2D-3D registration of a radiograph and a cone beam CT using line-segment enhancement," Med. Phys. **33**, 1398–1411 (2006).
[32]L. Lemieux, R. Jagoe, D. R. Fish, N. D. Kitchen, and D. G. Thomas, "A patient-to-computed-tomography image registration method based on digitally reconstructed radiographs," Med. Phys. **21**, 1749–1760 (1994).
[33]J. Weese, G. P. Penney, P. Desmedt, T. M. Buzug, D. L. Hill, D. J. Hawkes, J. Weese, G. P. Penney, P. Desmedt, T. M. Buzug, D. L. Hill, and D. J. Hawkes, "Voxel-based 2-D/3-D registration of fluoroscopy images and CT scans for image-guided surgery," IEEE Trans. Inf. Technol. Biomed. **1**, 284–293 (1997).
[34]G. P. Penney, J. Weese, J. A. Little, P. Desmedt, D. L. Hill, D. J. Hawkes, G. P. Penney, J. Weese, J. A. Little, P. Desmedt, D. L. Hill, and D. J. Hawkes, "A comparison of similarity measures for use in 2-D-3-D medical image registration," IEEE Trans. Med. Imaging **17**, 586–595 (1998).
[35]G. P. Penney, P. G. Batchelor, D. L. Hill, D. J. Hawkes, J. Weese, G. P. Penney, P. G. Batchelor, D. L. Hill, D. J. Hawkes, and J. Weese, "Validation of a two-to three-dimensional registration algorithm for aligning preoperative CT images and intraoperative fluoroscopy images," Med. Phys. **28**, 1024–1032 (2001).
[36]V. Baltzopoulos, "A video fluoroscopy method for optical distortion correction and measurement of knee-joint kinematics," Clin. Biomech. (Bristol, Avon) **10**, 85–92 (1995).
[37]J. Canny, "A computational approach to edge detection," IEEE Trans. Pattern Anal. Mach. Intell. **PAMI-8**, 679–698 (1986).
[38]D. E. Goldberg, *Genetic Algorithms in Search and Optimization* (Addison-Wesley, Boston, 1989).
[39]S. Forrest, "Genetic algorithms: Principles of natural selection applied to computation," Science **261**, 872–878 (1993).
[40]T.-W. Lu, T.-Y. Tsai, M.-Y. Kuo, H.-C. Hsu, and H.-L. Chen, "In vivo three-dimensional kinematics of the normal knee during active extension under unloaded and loaded conditions using single-plane fluoroscopy," Med. Eng. Phys. **30**, 1004–1012 (2008).
[41]P. J. Besl and N. D. Mckay, "A method for registration of 3-D shapes," IEEE Trans. Pattern Anal. Mach. Intell. **14**, 239–256 (1992).
[42]B. J. Fregly, H. A. Rahman, and S. A. Banks, "Theoretical accuracy of model-based shape matching for measuring natural knee kinematics with single-plane fluoroscopy," J. Biomech. Eng. **127**, 692–699 (2005).